Available online at www.sciencedirect.com
SCIENCE DIRECT®
ELSEVIER
Earth and Planetary Science Letters 211 (2003) 27–44
EPSL
www.elsevier.com/locate/epsl

A new seismic model of the Moon: implications for structure, thermal evolution and formation of the Moon

Philippe Lognonné *, Jeannine Gagnepain-Beyneix, Hugues Chenet

Institut de Physique du Globe de Paris, Département de Géophysique Spatiale et Planétaire, UMR7096-CNRS-IPGP-Université Paris VII, 4 Avenue de Neptune, 94100 Saint Maur des Fossés, France

Received 30 October 2001; received in revised form 20 December 2002; accepted 21 March 2003

Abstract

The seismic determinations of the crustal thickness and mantle velocities are key parameters for most geophysical and geochemical lunar studies. We determine a new seismic model of the Moon after a complete independent reprocessing of the Apollo lunar seismic data with determination of arrival times of about 60 natural and artificial lunar quakes, as well as travel times of converted phases at the crust–mantle interface below the Apollo 12 landing site. On the near side in the Procellarum KREEP Terrane, the only major discontinuity compatible with the crust–mantle boundary is located around 30 km deep. In this terrane, seismic constraints on the crust and mantle lead to a 30 km thick anorthositic crust and a pyroxenite cold mantle, with a bulk composition of 6.4% Al_2O_3, 4.9% CaO and 13.3% FeO. Mantle temperatures are in accordance with profiles obtained from the observed electrical conductivity and exclude a liquid Fe core, while being compatible with a Fe–S liquid core. Our Moon model might be explained by a mixture of a primitive Earth with tholeiitic crust and depleted upper mantle, together with a chondritic enstatitic parent body for the impactor planet. It provides mixture coefficients comparable to those obtained by impact simulation as well as an estimate of bulk U of about 28 ppb, in accordance with the U budget in a 40 km mean thick crust, 700 km thick depleted mantle and a lower undepleted primitive mantle.

1. Introduction

Lunar Prospector has provided a more detailed view of the lunar surface composition [1,2] and a new determination of the mean density and inertia factor [3]. The extrapolation of these results with depth depends strongly on the seismological measurement of the thickness of the crust and internal structure. From the analysis of the first seismic data in the 1970s, a crustal thickness of about 60 km near the Apollo 12 [4] landing site in the Procellarum KREEP Terrane (PKT) and 70 km near the Apollo 16 [5] landing site is generally assumed. This implies a proportionally much larger crustal volume than for the Earth reaching about 12% of the total volume compared to only 0.5% for the Earth. Recent independent studies of Khan et al. [6,7] and of our group [8], however, point toward a thinner crust in the range of 30–45 km.

This paper focus on the mineralogical implica-

* Corresponding author. Tel.: +33-1-45114264; Fax: +33-1-45114257.
E-mail address: lognonne@ipgp.jussieu.fr (P. Lognonné).

0012-821X/03/$ – see front matter © 2003 Elsevier Science B.V. All rights reserved.
doi:10.1016/S0012-821X(03)00172-9

tion of the re-analysis of Apollo seismic data in the upper mantle and the limits of such velocity models, especially in terms of their uniqueness. We confront geophysical and geochemical constraints and study the consequences of both a reduced crustal thickness and the mineralogical interpretation of the mantle seismic velocities on the formation and evolution of the Moon. Finally, we present new constraints supporting an enstatitic chondritic origin for the Earth's impactor which formed the Moon.

The Apollo crustal thickness of 60–70 km indeed leads to contradictions when combining other geophysical and geochemical constraints. These constraints were provided by Apollo for heat flux [12] and seismology [11], and by Clementine [13] and Lunar Prospector for gravity [3]. Geochemical constraints are either from Apollo sample analysis or from remote sensing, especially with respect to the bulk Al_2O_3, CaO, FeO and Th/U contents of the Moon. A first example is the bulk U content, as low as 19 ppb for the most recent analysis of the Apollo heat flux data [12]. This is in contradiction with previous higher estimates from heat flow of about 33–44 ppb [14,15] or with a more recent analysis of the Th content of the major lunar terranes [16] which allows an indirect computation of the U lunar bulk content to about 39 ppb when a mean crustal thickness of 70 km is taken.

A second example is the Al_2O_3 bulk content constrained by the composition and thickness of the highland plagioclase feldspar crust. The formation of such an aluminum-rich crust implies a crystal–liquid fractionation of a very large volume of the Moon, within a primitive magma ocean. A depth of 600 km is needed by geochemistry [14,15], while the scarcity of extension and compression features on the Moon has been used to propose 200 km as a depth upper limit [17], unless very large differentiation between crust and mantle occurs [18]. In the latter case, about 50% of the Moon volume could have been molten and greater depths are found.

As an alternative, an ad hoc two-layer crustal model was proposed on the basis of geochemical and remote sensing data [19], in which only the upper crust is anorthositic and primarily formed by the crystallization of a magma ocean, while the lower crust could have been formed later by magmatic processes. It is supported by the analysis of multiring basin ejecta, which indicates an increase of the amount of mafic ejecta with increasing basin size, and could be interpreted by a lower crust with noritic composition [19,20] or by a zoned crustal composition related to the crystallizing magma ocean [21]. Such a two-layer model for the crust can explain gravity data [22] but no major discontinuity in the crust is detected by seismic data [4–7,23]. Gravity analysis also suggest that any lower crust might be very strongly thinned and even disappear beneath some major impact basins on the far side [22]. But lateral density variations in the upper mantle, suggested from Clementine remote sensing analysis [16], could also be used to explain the gravity field [22].

Before the Lunar A [24] new data, we propose to improve the view of the lunar crust and mantle by reprocessing the Apollo seismological data and taking the Lunar Prospector gravity constraints [3]. Our study does not confirm the 60 km value of the crustal thickness in the PKT terrane, which is found in the range of 30 ± 2.5 km, leading to a mean crustal thickness of 40 km. New geophysical constraints on the lunar composition and formation are then proposed.

2. Reprocessing of the Apollo seismic data

We reprocessed the seismic data produced between 1969 and 1977 by the Apollo seismometers [4,11]. The picking of the arrival times was done by one of us (J.G.B.) with particular attention devoted to the estimation of uncertainties and by associating with P and S arrival an error of 1, 3 or 10 s. See Fig. 1 for an example of typical data with P/S arrival times. This first stage was done without reference to the previously published arrival times and also included the deep tidally triggered events [25], stacked after time alignment relative to a reference event. All relocated events are listed in Tables 1–4, together with arrival times and errors. The mean error in the arrival times used in the inversion is found to be about 2 s. In total, 59 events were kept for the

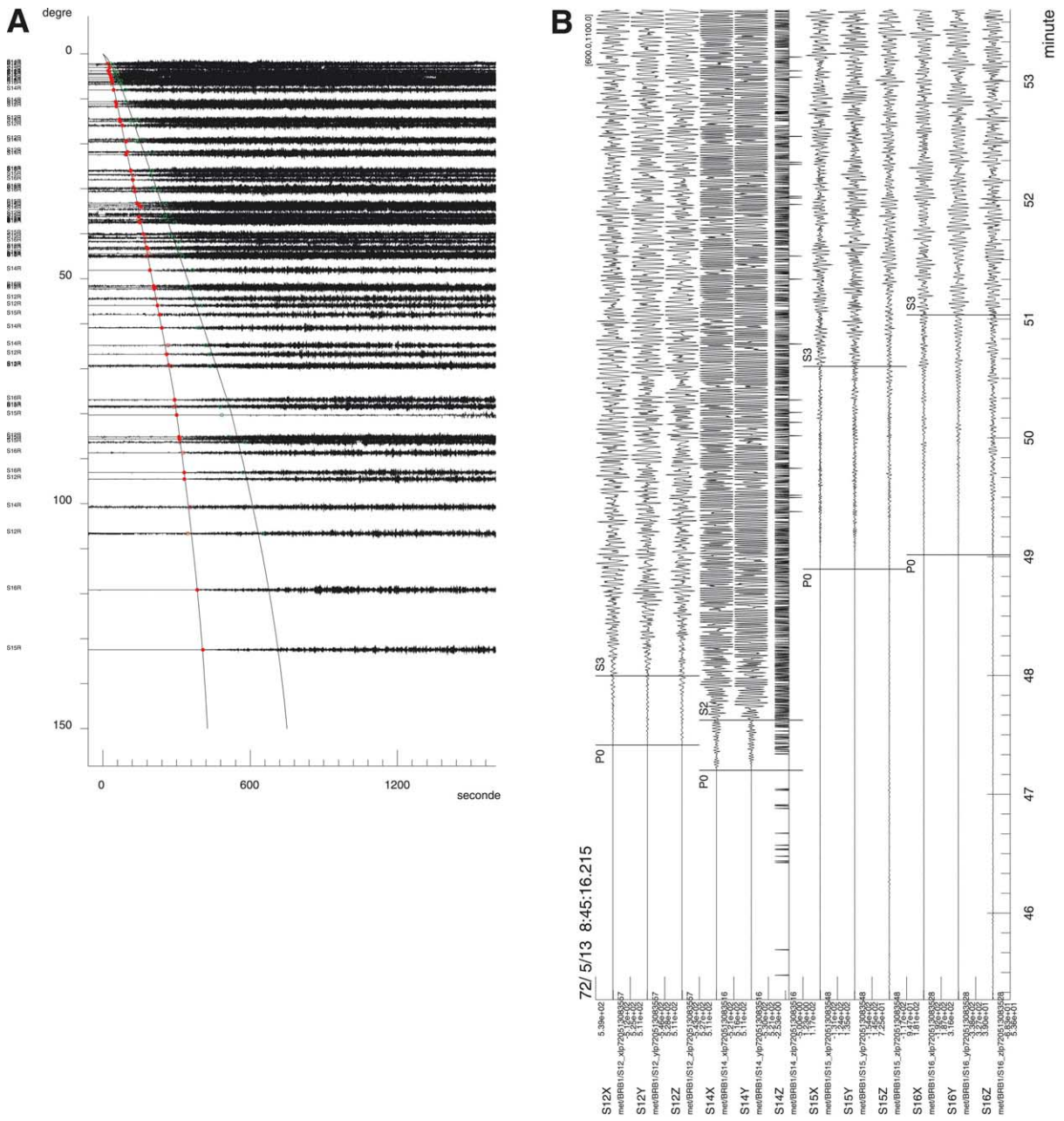

Fig. 1. (A) Profile of the meteoric and artificial events at the stations Apollo 12, 14, 15, and 16 on the radial component. Records are data from the LP seismometer, most of the time from the peaked output. Circles indicate the arrival times. Solid ones are for σ smaller than 3 s. The solid lines show the P and S hodochrones corresponding to Nakamura's model [26]. (B) Example of travel time determination for a typical meteorite impact recorded by the network on May 13, 1972. Detection is done at four stations, providing eight arrival times and therefore four data useful for the seismic model determination after localization of the impact. P0-S0 indicate readings with less than 1 s of error while P1-S1, P2-S2, and P3-S3 are for 3 s, 10 s, and more than 10 s respectively. P3-S3 readings were not used in the determination of the model.

Table 1
List of the artificial impacts used in the inversion

Type	Lat.	Long.	Depth	ϕ	a	b	c	Date/hour/min	Seconds	Error	P12		P14		P15		P16		S12		S14	S15	S16
12LM	−3.94	−21.20	0	0	0.0	0.0	0	6911202217	17.70	0.0	42.4	2							56.29	2			
13S4	−2.75	−27.86	0	0	0.0	0.0	0	7004150209	41.00	0.0	68.8	0							89.04	2			
14S4	−8.09	−26.02	0	0	0.0	0.0	0	7102040740	55.40	0.0	90.8	0											
14LM	−3.42	−19.67	0	0	0.0	0.0	0	7102070045	25.70	0.0	46.8	1	44.5	1									
15S4	−1.51	−11.81	0	0	0.0	0.0	0	7107292058	42.90	0.0	97.0	1	79.7	0									
15LM	26.36	0.25	0	0	0.0	0.0	0	7108030303	37.00	0.0					64.5	0							
16S4	1.30	−23.80	0	0	0.0	0.0	0	7204192102	04.00	0.0	31.4	0	47.5	0	150.9	0							
17S4	−4.21	−12.31	0	0	0.0	0.0	0	7212102032	42.30	0.0	98.0	0	74.5	0	196.5	1	164.2	0					

Column 1 is type of event, and columns 2–4 are latitude, longitude, and depth respectively. ϕ is the orientation of the semi-major axis of the ellipse error with respect to east–west, in degrees, and a and b are the semi-major and -minor axes of the ellipse error in km, c is the error in depth. Column 9 provides the event time in years, month, day, hours, and minutes, 10 the event time in seconds, 11 the error in event time, 12–13, P arrival time at Apollo 12 and error, 14–15, 16–17, 18–19 the same for Apollo 14, 15, and 16 respectively, 20–21 S arrival time for Apollo 12 and error, 22–23, 24–25, 26–27 the same for Apollo 14, 15, and 16 respectively. Error code is 0, 1, 2 for error smaller than 1 s, 3 s and 10 s respectively. Fifteen P arrival times and two S arrival times provide a total of 17 data for structure.

Table 2
List of the 19 meteorite impact events used in the inversion

Type	Lat.	Long.	Depth	ϕ	a	b	c	Date/hour/min	Seconds	Error	P12		P14		P15		P16		S12		S14		S15		S16	
M	74.10	2.60	0	16	2.7	1.1	0	7201040631	19.72	1.7	318.0	2	315.0	1	215.0	1			542.0	2			350.0	1		
M	1.50	−17.10	0	−52	0.3	0.2	0	7205130845	39.49	1.0	84.9	0	72.1	0	173.5	0	181.0	0			97.5	2				
M	32.80	137.60	0	−47	1.3	1.1	0	7207172150	57.90	4.4	473.7	0	483.0	0	418.2	0	445.8	0								
M	24.00	10.10	0	−7	0.7	0.3	0	7207311808	15.72	2.3	193.4	1	174.7	0	52.6	0			285.0	2			82.0	1		
M	15.80	22.90	0	20	2.9	1.6	0	7208292258	33.57	3.5			210.0	2	132.0	2	145.0	2			344.0	2	190.0	2		
M	28.70	41.10	0	39	4.1	2.4	0	7309262046	16.32	4.5	295.0	2	280.0	2	155.0	1	192.0	2					255.0	2		
M	−24.80	−25.10	0	59	5.2	1.8	0	7312241003	19.35	4.5	119.0	1	113.0	1	250.9	1	190.0	2								
M	7.40	−33.60	0	−5	2.2	0.9	0	7404191830	03.27	1.8	70.9	1	97.0	1	168.3	1	209.2	0								
M	20.30	6.50	0	9	0.8	0.6	0	7407171205	02.89	3.7	153.4	1	148.7	1	40.6	1	132.1	1					69.0	2		
M	−7.30	19.90	0	52	1.0	0.7	0	7411211315	40.79	2.2	222.9	1	193.0	1	182.7	2	70.5	0								
M	1.60	−8.20	0	−85	1.3	0.5	0	7412150907	15.17	3.8	95.1	1	66.6	1			128.1	1			109.3	2	208.2	2		
M	−52.40	4.20	0	−77	4.0	2.3	0	7503052149	22.30	7.2	236.1	2	225.0	2			209.7	2	398.0	2					330.0	2
M	2.00	43.20	0	−11	4.5	0.5	0	7504121812	38.22	0.7	298.1	0	277.8	1	220.6	0	162.1	1								
M	−36.40	−121.30	0	−47	3.3	1.1	0	7505040959	28.99	2.3	360.6	0	376.1	0	436.0	1	413.0	0								
M	−39.40	62.80	0	55	2.7	2.0	0	7601130711	22.80	6.0	332.7	1	338.1	2	333.8	1	236.0	1							357.9	2
M	−16.80	−10.00	0	67	2.0	0.6	0	7605280601	56.38	5.4	163.7	2	126.5	1			169.0	1	216.0	2	169.0	2	373.0	2		
M	23.80	−73.90	0	37	1.8	0.8	0	761142313	06.67	0.9	228.6	0	246.9	0	273.8	1	337.7	0								
M	−20.50	−63.80	0	23	1.8	0.8	0	7704712332	06.03	0.7	183.7	1	197.8	1	306.4	0	298.2	0								
M	−13.50	−75.30	0	−84	7.7	3.1	0	7706282222	31.17	3.8	239.9	1	250.0	2	344.0	2	358.5	2	390.0	2						

Same convention as for Table 1. Seventy P arrival times and 18 S arrival times provide a total of 31 data for structure.

Table 3
List of the eight shallow moonquake events used in the inversion

Type	Lat.	Long.	Depth	ϕ	a	b	c	Date/hour/min	Seconds	Error	P12		P14		P15		P16		S12		S14		S15		S16	
SH	12.80	51.00		−20	2.9	109	109	7209171435	03.00	2.5			278.0	2	186.0	1	170.0	2			460.0	2	322.0	2	285.0	2
SH	48.00	38.20	10	58	3.2	110	110	7212062308	33.40	7.4			302.0	2	167.0	2	280.0	2			507.0	2	278.0	2	430.0	2
SH	21.90	82.60	2	−10	2.4	63	63	7407110046	18.26	1.3	377.1	1	365.4	2	296.0	2	297.7	0	655.9	2			485.1	2		
SH	26.10	−92.70	0	42	2.4	38	38	7501030141	58.36	6.8	334.3	1	350.8	1	363.1	1	434.9	1	543.0	2	581.0	2	608.0	2	730.0	2
SH	64.10	59.90	0	59	1.8	14	14	7501120313	51.74	0.6			360.0	2	260.0	2	350.0	2	612.9	2			400.0	0	567.6	0
SH	−17.00	−26.10	21	44	3.0	112	112	7502132203	50.78	0.7			117.9	1	248.0	2	210.0	2	154.4	2	167.8	2			321.7	2
SH	44.10	34.00	125	76	3.2	179	179	7601041118	54.92	0.3			298.0	2	175.1	2	262.0	1			474.0	2	259.0	2	412.0	2
SH	52.50	−25.80	185	−24	1.2	51	51	7603061012	22.08	2.0	236.9	1	233.2	0	158.6	1	282.6	1	381.30	1	387.7	1	251.2	2	466.1	2

Same convention as for Table 1. Twenty-seven P arrival times and 25 S arrival times provide a total of 20 data for structure.

model exploration: 27 impacts, including eight artificial impacts (Tables 1 and 2), eight shallow quakes (Table 3) and 24 deep quakes (Table 4). Other quakes were rejected: they were constrained by four or fewer arrival times with acceptable errors which is just enough for the quake position and time source. Fig. 1A illustrates the data set with a seismic profile of the meteorite impacts with increasing epicentral distances. The range of epicentral distances for useful arrival times varies from a few degrees to about 130° for P arrival times and to about 75° for S ones. The deepest useful rays sound the lunar interior down to a radius of about 400 km for P and 600 km for S (see also Fig. 9). Only geodetic data therefore constrain any Moon core smaller than about 500–600 km. Due to the location of the Apollo network, our data set mainly constrains the crustal thickness of the near side of the Moon for the PKT.

The maximum number of data per event is eight (P and S arrival times at four stations, with moreover two stations almost 200 km apart) but most of the time, the arrivals on some stations are too noisy to be read with a useful error: for the 59 events studied, we can use only 318 P and S

Table 4
List of the 24 deep moonquake events used in the inversion

Type	Lat.	Long.	Depth	ϕ	a	b	c	Date/hour/min	Seconds	Error	P12		P14		P15		P16		S12		S14		S15		S16	
A01	−17.40	−38.40	917	−25	1.1	0.6	11	7309300410	58.84	0.8	192.4	0	194.8	0	251.0	0	239.7	1	290.5	1	300.6	2	396.8	0	377.8	2
A06	49.70	54.70	860	74	1.0	0.7	11	7607021052	25.31	2.6	259.4	0	258.2	0	191.6	0	235.2	0	444.7	0	433.3	1	316.9	1	377.9	1
A07	24.00	53.70	900	−75	0.8	0.7	12	7607020311	24.18	0.6	251.2	0	242.0	0	191.4	0	198.8	1	426.1	1	408.2	0	314.5	1	332.4	1
A08	−28.00	−28.10	940	51	2.0	1.2	21	7705161052	29.35	3.0	173.2	1	174.0	1			189.9	1	270.5	1	276.3	0			328.9	1
A09	−37.80	−30.80	975	14	4.0	2.6	43	7704161958	04.27	0.9	167.5	2	159.7	1				0	277.1	0	277.7	1	377.1	2	320.3	2
A11	9.30	17.50	1200	−42	0.8	0.7	12	7706180501	16.06	0.7			192.2	2	173.2	1		0	329.3	0	319.8	0	299.4	0	296.4	0
A14	−28.70	−33.90	880	50	1.7	1.3	22	7305281853	12.96	1.3	149.7	1	152.5	1			191.0	1	254.8	1	260.5	1	370.1	1	319.7	1
A16	6.80	5.10	1105	9	1.2	0.7	18	721081524	35.48	0.4			184.5	2	185.4	1	185.4	1	315.2	1	305.5	1	298.6	0	298.3	1
A17	23.10	−18.00	861	−47	2.6	0.4	15	7211070852	07.94	0.6	143.0	0	141.9	1	133.3	2	178.0	1	246.2	1	243.9	1	228.9	0		
A18	18.60	34.70	882	−67	1.8	0.9	24	7301052250	30.86	1.5	229.2	2	216.2	0	188.5	2	188.5	1	373.2	1	357.5	0	276.5	1	279.6	2
A20	21.70	−41.00	1055	−1	2.4	0.8	13	7205151718	07.15	1.2			179.9	2	174.3	0	204.5	0	279.2	0	284.1	1			357.3	1
A24	−36.80	−38.90	980	57	2.1	1.7	32	7706121817	38.54	0.3	196.7	1	198.0	1				2	315.8	2	319.7	0	417.8	2	368.0	1
A25	34.40	59.30	898	87	2.0	1.7	26	7706092015	07.55	1.8	241.3	2	242.1	1	179.2	0	200.7				409.3	1	312.7	1	345.6	2
A27	22.50	18.50	1059	−24	1.9	1.4	14	7705160001	51.54	1.3			236.1	2	193.4	0	205.9	2	366.0	2	352.3	1	299.9	0	338.9	2
A30	11.80	−34.30	921	−37	1.5	1.0	23	7205170042	45.93	0.5			181.0	0	201.7	1		1	273.3	1	283.4	1	321.4	1	365.2	1
A33	6.90	117.80	887	−9	1.5	1.3	30	7210111935	46.79	1.1	369.9	2	349.1	0	318.0	0	311.8						528.1	1	511.5	1
A34	7.00	−9.30	932	−32	1.2	0.6	26	7206141834	27.24	2.6	154.9	1	158.1	1	164.4	1		1	249.8	1	256.5	1	265.2	0	279.3	1
A40	−1.60	−10.90	886	−80	1.2	0.7	23	7306272348	35.37	0.6					185.0	2	173.1	0	247.9	0	242.6	1	286.7	1	277.8	1
A41	13.90	−26.80	953	−28	5.6	2.2	84	7206081616	24.70	3.5			163.4	2	172.4	2		2	247.3	2	270.1	2	284.1	1	325.6	2
A42	22.70	−53.50	1004	−53	1.8	1.4	24	7305030152	35.84	2.2	195.8	1	205.6	0	229.9	2	245.6	1	318.9	1	331.9	1	352.5	1	418.0	1
A44	51.90	57.10	956	−74	5.8	1.9	20	7405190309	04.66	1.3			235.4	1	177.6	1		2	434.9	2	411.4	0	307.4	1	376.2	2
A50	9.40	−51.60	835	−13	2.4	1.5	30	7304300105	26.01	3.7	174.2	2	174.2	1				2	292.0	2	285.0	1	348.1	1	397.8	1
A51	8.80	15.70	888	−28	1.1	0.5	22	7402180835	27.40	1.2			181.2	2	149.0	2		2	320.7	2	291.1	0	254.1	0	248.8	1
A97	−3.40	18.70	1000	−3	2.8	2.3	25	7705190608	21.53	2.1			180.6	1	173.8	1	156.0	2	310.3	2	295.2	2	301.1	2	251.8	1

Same convention as for Table 1. The date is for the reference event used in the stack of all deep events associated with the same focus. Seventy-one P arrival times and 91 S arrival times provide a total of 66 data for structure.

arrival time readings with a sufficiently small error (about 5.4 data per event). For shallow and deep quakes, four parameters are needed for the source determination. Three are needed for meteorite impacts. Without the degree of freedom related to the source positions and time, we have therefore a set of 134 constraints on the interior structure. Two alternative analyses are possible: the first one, chosen by Khan et al. [6,7], uses a large number of layers (about 50) with two unknowns per layer, V_p and V_s. The mean a priori error will then be more or less transferred without reduction on the a posteriori errors, typically between ± 350 m/s and ± 750 m/s at large depth [7]. Such errors are too large for mineralogical interpretations [10]. The travel times, however, accumulate the slowness along the ray and integrate naturally the structure and we prefer to invert the mean velocities of a limited number of layers. Tests led us to consider nine layers and therefore 18 inverted parameters as a good compromise between depth and velocity resolution. This reduces the error by about 2.7, leading to an a posteriori error of ± 125 m/s, a minimum value for mineralogical interpretations. We tested the position of layers by adding thin layers of 5 km above and below or reducing their width, while limiting the parameter numbers by fixing the V_p/V_s ratio. The error for the depth of discontinuities is related to the thickness of the test layers and is therefore ± 2.5 km. Discontinuities in the upper part of the Moon (first 100 km), including the crust–mantle discontinuity, are robust and were retrieved with tests using more layers. In the lower mantle, the depth of discontinuities (if present) is not well resolved.

Arrival times weakly constrain gradients in the crust and we also used the S-receiver function method [23] to detect crustal conversions at the Apollo 12 landing site. We used 13 deep focus events (A5–A10, A14, A18, A20, A21, A30, A40, A42). For each nest, a tidal periodicity of activity [25] occurs and the related signals were stacked to enhance arrival time reading. We then deconvolved in the time domain the R and Z components of each stack by the R component of the S wave, the latter looking like a 'bump' after deconvolution. The receiver function obtained by a last stack is shown in Fig. 2. The M-shaped phase arriving about 8 s before the S arrival is a S to P converted phase from the mantle–crust transition. This additional constraint was used in the inversion. A conversion was, however, detected only at station Apollo 12 where site effect amplifies seismic signals [23].

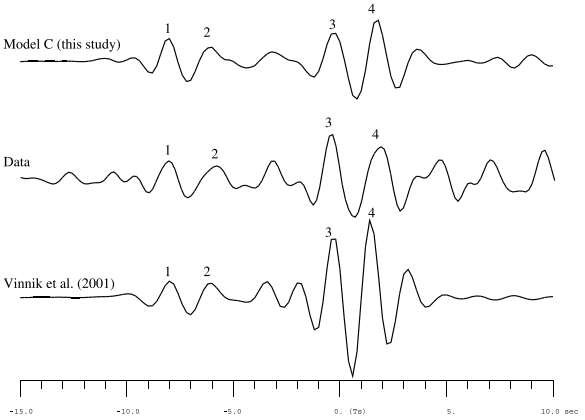

Fig. 2. Observed and modeled receiver function below Apollo 12. The receiver function shows waves associated with conversions of the S body wave packet. Signals are low-pass filtered data with a corner period at 1.2 s. The main converted phase is a conversion from S to P at the bottom of the crust arriving about 8 s before the S wave. The observed receiver function is in the center. The bottom trace was obtained with a model from Toksoz et al. [4] and Vinnik et al. [23] with a crustal thickness of 60 km. The top trace was obtained with model C derived from model B, with a crust discontinuity at about 27 km for P waves while a gradient in S waves extends up to about 40 km depth. It provides $T_{Sp}-T_S$ and a better fit in amplitude. Models B and C are shown in Fig. 5.

We then determined the best seismic velocity models by using the complete data set with and without the arrival time of the S to P conversion. We searched a class of acceptable models by a systematic exploration of model space, each of them being associated with the a posteriori variance defined as:

$$V = \sum_{Pi} \frac{(t_{Pi}^{obs} - t_{Pi}^{cal})^2}{\sigma_{Pi}^2} + \sum_{Si} \frac{(t_{Si}^{obs} - t_{Si}^{cal})^2}{\sigma_{Si}^2} + \frac{(t_{Sp}^{obs} - t_{Sp}^{cal})^2}{\sigma_{Sp}^2}$$

where t_{Pi}^{obs}, t_{Si}^{obs}, σ_{Pi}, σ_{Si}, t_{Pi}^{cal}, t_{Si}^{cal} are the observed arrival times, Gaussian errors and computed arrival times for the ith data of P and S respectively

and t_{Sp}^{obs}, σ_{Sp}, t_{Sp}^{cal} are the same for the Sp travel time. We limited the possible models by constraining the V_p/V_s ratio to range from the normal value of 1.7 to values as high as 2, convenient for highly fractured materials. We also prohibited models with decreasing velocity with depth in the crust. This operation was done in two steps: an exploration with only impact data, looking for information for the crust, and a global exploration inversion with all the data, sampling especially the mantle. For each model a model probability was computed assuming a Gaussian error and the velocities were explored in each layer with an interval of 250 m/s. While reducing the number of layers, the method used is therefore more robust than more classical inverse problems in the sense that it covers a much wider space of models.

3. Results

We focus this paper on the results in terms of structure. Other results will be presented in another paper (Gagnepain-Beyneix et al., in preparation). Ten million combinations were tested for the crust and two million for the deeper structure. The best model is named model A and appears as a solid line in Figs. 3 and 4. The details of the results in terms of misfit are shown in Table 5. The sensitivity of arrival times to the crustal thickness is, however, weak: the misfit of model A, for which a 30 km crust is found, is only slightly better by about 0.1–0.2 s than the 60 km crust models of Nakamura [26] and Goins et al. [27]. This difference is marginal when compared to the mean error of 2 s found on the data. A new inversion with the conversion travel time in the crust, more sensitive to the crust structure, was therefore performed leading to model B. Travel times, however, give the mean velocity in a layer and do not allow discriminating between a continuous increase or sharp interfaces. We there-

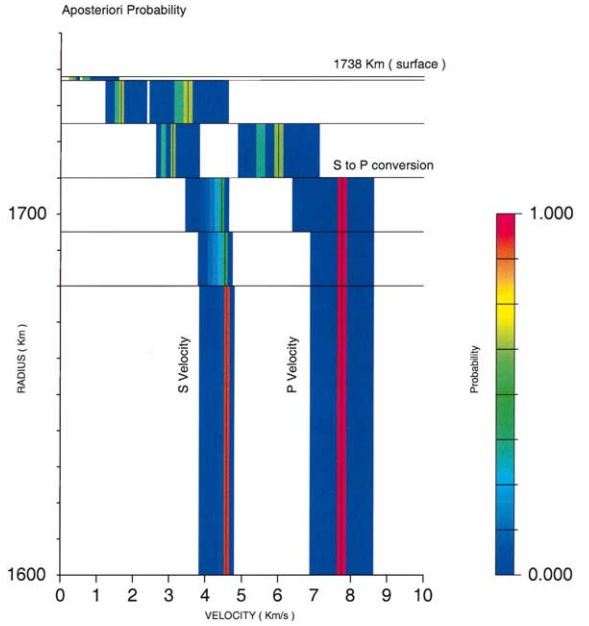

Fig. 3. A posteriori mean velocity probability in the crust with a $T_{Sp}-T_S$ value of −8 s when generated by the 28 km deep discontinuity. The probability of a given velocity value in a layer is the sum of probabilities of all models with this value in this layer. The black line represents the most likely model. Only impacts were used for this model, limiting therefore the number of unknowns to three for the source (latitude, longitude, and time).

Table 5
A posteriori variance (in seconds) for different models using the different arrival times data set (rows 2–7)

Model/data (number)	Goins [27]	Khan [6]	Nakamura [26]	Toksoz [4]	A	B	C
Art. impacts (8)	2.72	3.3	2.76	3.91	2.33	2.46	2.59
All impacts (27)	2.49	3.2	2.56	3.37	2.38	2.44	2.50
Near impacts (20)	2.48	3.8	2.39	3.44	2.37	2.21	2.52
Deep+shallow (35)	1.57	3.3	1.70	2.41	1.57	2.42	2.45
Deep (24)	1.56	3.2	1.49	1.73	1.45	1.46	1.49
All (59)	1.98	3.26	2.07	2.82	1.93	1.95	1.97
$T_{Sp}-T_S$	−8.6	−9	−8.6	−8.2	−6	−8	−8

Row 8 is the $T_{Sp}-T_S$ for the crustal boundary. Variance is smaller than or comparable in general to [27], and much better than models from [6], [4] and [26]. The mean error for all data is about 2 s and is close from the final variance of models A, B, and C.

fore did a last test by modifying model B with gradients in the crust compatible with both the travel times and the conversion amplitudes (model C, see Fig. 5). Our three models all have a 30 km crust, and their misfits are generally better than those obtained for previously published ones (Table 5). Moreover, model C fits the amplitude of the receiver function much better than a similar fit using a 60 km crustal [23] model. Even by imposing the Sp−S travel time to come from a deeper interface and searching models with discontinuities at 60 km, we did not find any discontinuity at that depth compatible with both the travel time and the conversion.

4. Crustal structure and thickness

As shown in Fig. 3, a discontinuity (or rapid gradient within 5 km) is found at a depth of 30 ± 2.5 km and is proposed as the crust–mantle interface. This is shallower than the depth of 35–45 km of Khan et al. [7]: tests with Nakamura's data set indicate that the difference could be associated with the different data and data error weight (Gagnepain-Beyneix et al., in preparation). Anyway, these two values are much smaller than the 60 km found by the other seismic studies [4,5,26,27]. A smaller discontinuity is also observed for S at that depth. The V_p/V_s ratio decreases from high values around 2 in the first 30 km to the standard value of 1.73 below 45 km suggesting that the velocity profile reflects fractures of the medium rather than possible compositional changes [28,29]. Possibly, the slightly lower depth of the major discontinuity observed in the S wave velocities when compared to the P wave profile reflects some continuation of the impact-induced cracks below 30 km, i.e. deeper than the previously proposed 25 km depth [30]. However, the S velocities have large errors in the crust due to the low number of high quality S arrival time data, a consequence of scattering. These features are therefore within the uncertainties and a constant S velocity might be possible too. All seismic data we used favor a crust–mantle discontinuity at a depth around 30 km in the PKT. The large a posteriori velocity errors in the transition zone

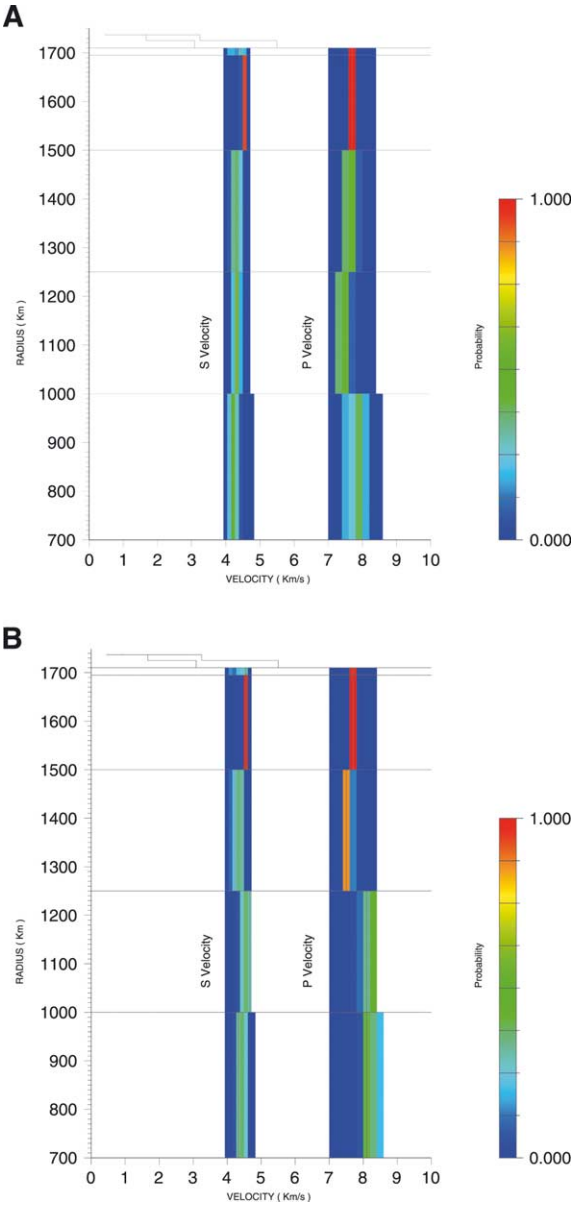

Fig. 4. (A) Same as Fig. 3 for the mantle structure. All quakes were used for this model. (B) Same as Fig. 3 for the mantle structure but without the five meteorites or shallow quakes sounding the deepest structure.

(and also in the crust) observed in Fig. 3, including the bimodal distribution at depth 15–28 km, may suggest large lateral velocity variations: this might reflect either velocity changes related to impact fractures, serial magmatism taking place

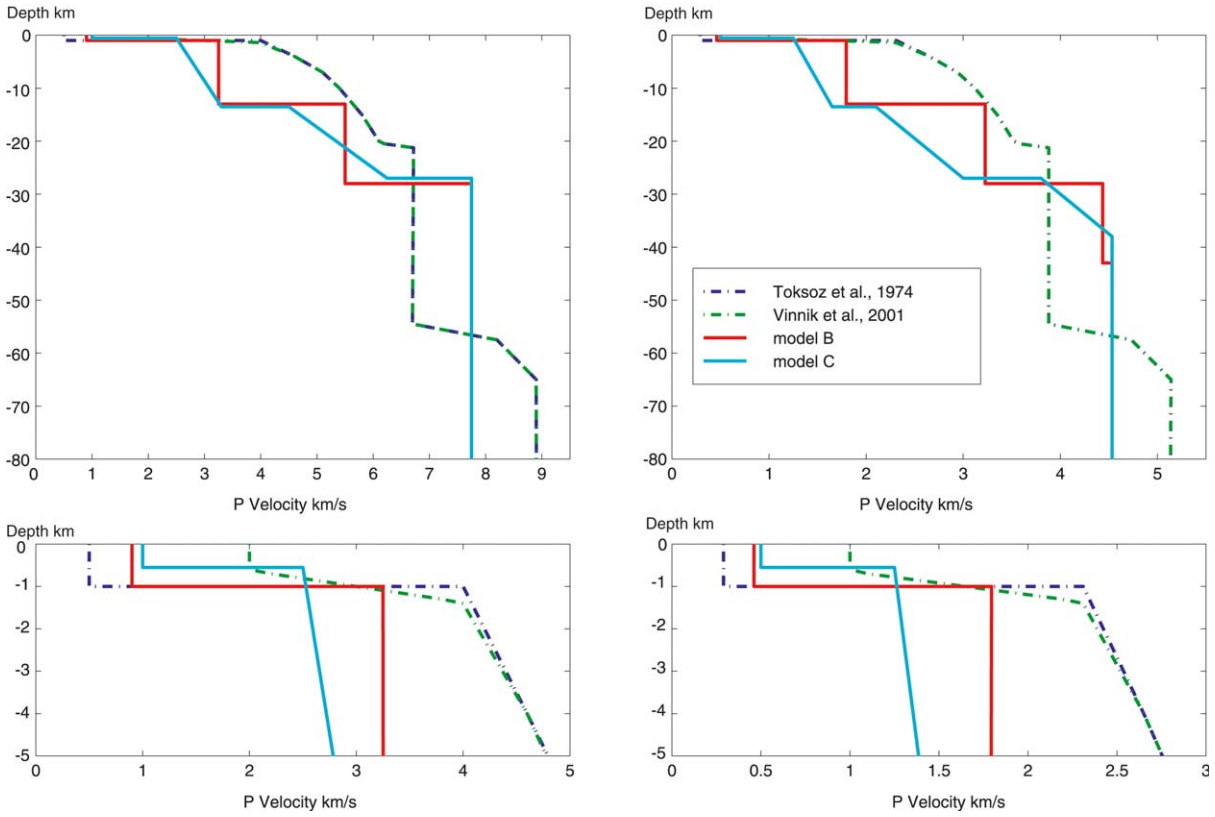

Fig. 5. Close-up of the crustal structure found in this study (models B and C) compared to other structures with a crustal thickness of 60 km. Model B is constrained by the arrival times only either of direct P and S body waves or crustal conversion from S to P. Model C is also constrained by the amplitudes of the receiver function.

after crust formation and through the fractures produced by impact cratering or the fact that seismic data are sampling different terranes of the Moon. Although an estimate of the mean planetary crustal thickness will need joint constraints of seismic and gravity data as well as the elevation of the Apollo landing sites we assume here an overall reduction of the crustal thickness by as much as 30 km for our model (20 km for the Khan et al. value [7]), leading, as we will show below, to a mean crustal thickness of the Moon in the range of 40 km when the other terranes are taken into account [16].

5. Upper and middle mantle structure

In the upper mantle, P and S velocities are about 7.75 km/s and 4.5 km/s respectively, close to values determined by Goins et al. [27] but different from the ones of Nakamura [26]. Other features are observed for the deep structure (Figs. 4A and 6), such as a slight velocity decrease with depth and an increase below 750 km depth (i.e. 1000 km in radius) of the mean velocity. We do not find any P velocities much higher than 8.5 km/s, confirming the range of values found in most previous studies. This is a major difference with the Khan et al. models [6,7], for which the 99% credible intervals below 700 km are centered at velocities higher than 10 km/s, pointing out, as noted by Khan et al. [7], more the ill-determined nature of seismic velocities at these depths than any mineralogical information. We also do not find a low shear velocity zone in the middle mantle, with its base at 500 km depth as in Nakamura

[26], which was interpreted as a distinct layer in the lunar middle mantle, but rather a continuous decrease of P velocity down to about 750 km depth, where we observe an increase of the P velocity. As the pressure is low in the lunar mantle, the effect of temperature increase dominates on the seismic profiles and can produce this velocity decrease, as pointed out by Goins [27].

Tests have shown that the velocities found in the upper mantle down to a depth of 500 km are stable to within ±150 m/s for several inversions with smaller velocity spacing (Gagnepain-Beyneix et al., in preparation). Together with the search strategy, this allows us to confirm a 3σ error of about ±150 m/s for these depths. The resolution of the seismic data set returned by the Apollo mission is, however, very poor concerning the lower mantle. Let us for example consider the P velocity increase obtained at a depth of 750 km in Fig. 4A. If we do not enter into the data set the five deepest quakes, we get another model (Fig. 4B), closer to Nakamura's model [26]. Our conclusion is that any deep discontinuity, if existing, is very poorly constrained by the Apollo data set and must be interpreted with care in terms of mantle structure. An overall increase of the seismic velocities between 500 and 800 km depth is, however, likely, either gradual or as a discontinuity. The determination of its depth is, however, strongly model- and event-dependent.

We now focus on the model interpretation in the upper mantle of the Moon, i.e. the first 500 km (Fig. 4A). We compare first the seismic velocities with eight mantle models proposed by various authors [31–35] all listed by Kuskov [31] (Fig. 6). In order to select among these models, we allow the mantle temperature to change and compute the misfit between the thermally shifted P and S profiles and our velocity model in the upper mantle. We take a mean relative temperature sensitivity for V_p and V_s of 1% for 100°C of temperature shift, close to the mean value obtained by Kuskov [31] for model 5. This sensitivity may of course depend on the mineralogy and be different for P and S velocities, but the typical errors of velocities in the upper mantle prevent us from any detailed analysis. We also take the constraints from magnetic sounding [38] (see Fig. 8), which typically provide a range of +100°C/−600°C with respect to the 900°C taken by Kuskov [31] at a depth of 400 km.

Models 1–4 need velocities smaller by 2–5%, especially for P, and therefore temperatures exceeding the magnetic sounding upper constraints. Model 8 needs 7% higher velocities and has to be colder than the lowest temperature. Three models remain and we focus on the two models (5 and 7) closest to our velocity profile, the last one needing a temperature change twice higher and close to our limits. These models correspond to two class of pyroxenite models, with either a low FeO content of about 14% and Al_2O_3 and CaO contents of 5.1% and 4.1% respectively (model 5 of Fig. 6, now defined as model I) or more FeO and less Al_2O_3 and CaO (model 7 of Fig. 6, now model II). As developed below, we prefer model I for both geochemical and geophysical reasons. Model I, proposed by Ringwood and Essene [35], is con-

Table 6
Comparison between the obtained density and seismic velocities and those of model I or model II (models 5 and 8 from [31])

Geophysical parameter	Model I	Model II
Mantle density at 900°C/400 km (kg/m^3)	3365	3454
Shear velocity at 900°C/400 km (km/s)	4.437	4.436
Bulk velocity at 900°C/400 km (km/s)	7.591	7.68
Mantle density at 285–410 km (kg/m^3)	3378	3378
Shear velocity at 285–410 km (km/s)	4.50	4.50
Bulk velocity at 285–410 km (km/s)	7.75	7.75
Mantle density temperature Shift (°C)	−65	+380
Shear velocity temperature Shift (°C)	−280	−365
Bulk velocity temperature Shift (°C)	−215	−95
Least square temperature Shift (°C)	−225	−140
Residual after temperature shift (%)	0.55	2.23

The residual is the square root of the sum of squared differences between the inverted value and model values, when corrected for the temperature by a least square fitting.

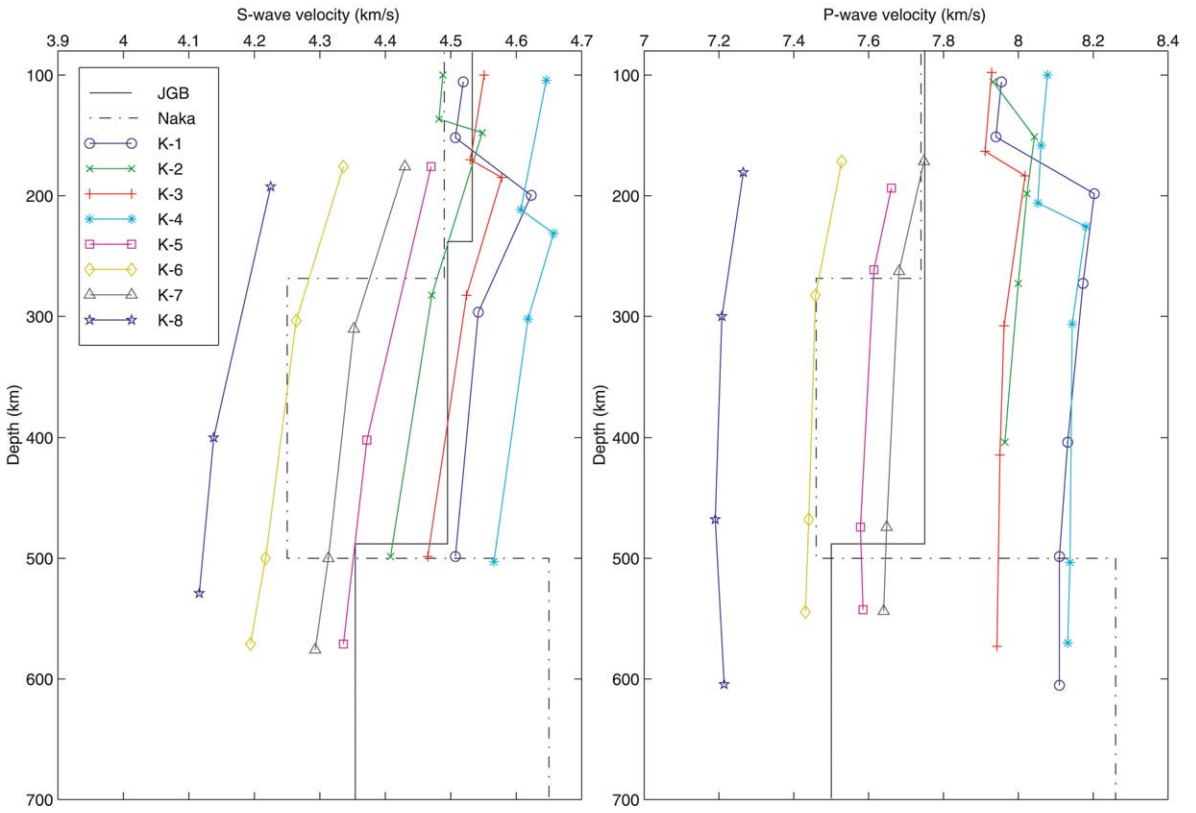

Fig. 6. Plot of the seismic velocities for different models, as compared to the velocities of Fig. 4A (continuous line). 220 m/s and 390 m/s in S and P velocity, respectively, correspond to about 500°C in temperature shift for model 5. See details of composition in table 2 of Kuskov [31]. Model 1 is an Al- and Ca-rich composition [32], model 2 is a Fe-rich composition [33], model 3 an intermediate model with orthopyroxene [33], model 4 a pyrolite composition [34], model 5 a model of lunar pyroxenite constrained by the source of mare basalt at depths of 200–500 km [35], and models 6–8 are pyroxenite models satisfying the mean velocity the upper velocity bound and lower velocity bound of the Nakamura model [26] obtained by Kuskov [31]. For models 5 and 7 we need the smallest temperature change.

strained by the composition of mare basalts at depths of 200–500 km. Extrapolating the chemical composition of model I in the mantle, we find a bulk composition of the Moon's mantle+crust of 53.5% SiO_2, 6.4% Al_2O_3, 13.3% FeO, 21.9% MgO and 4.9% CaO for a 40 km crust with composition provided by Taylor [15]. This value, close to the 13% bulk FeO found by Jones and Hood [36] or Mueller et al. [37], might, however, be affected by a lower mantle with a different composition.

Independent density constraints on the lunar interior [3] also favor model I instead of model II. The relevant measurements are the mean density, mean radius and inertia factor of $\rho = 3343.7 \pm 0.3$ kg/m^3, $a = 1738$ km and $I/Ma^2 = 0.3931 \pm 0.0002$ [3]. We model the Moon with four layers: a homogeneous crust, a transition layer in the upper mantle, a mantle and a core. The transition zone corresponds to a possible density gradient between the mantle and the crust. More complicated models may fit the data better but are much less resolved. The results for the mantle are shown in Fig. 7, and obviously depend on the crustal thickness as well as on a possible transition zone in the uppermost part of the mantle. We compute the mean crustal thickness by taking into account the different terranes of the Moon whose densities and surface fractions are given by Jolliff et al. [16]. For a PKT thickness of 60 km, we have a lunar crust density of 2920 kg/m^3 and a mean

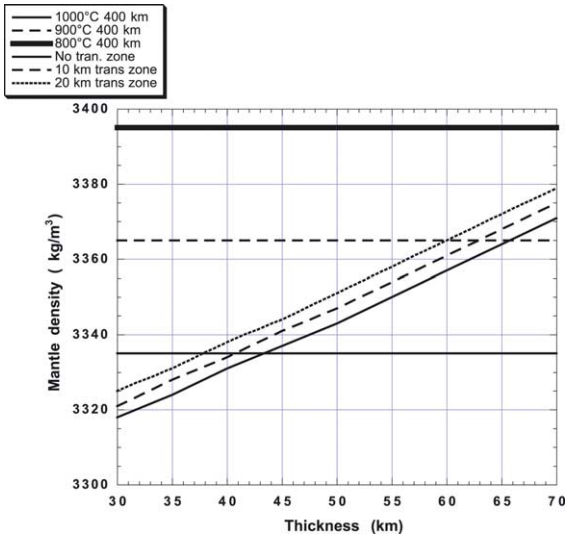

Fig. 7. Mantle density found for three different models with respect to crustal thickness. The two unknowns (mantle and core density) are found from the two data (mean density and inertia factor) assuming values for the crust density, thickness, and core size. Crust density is 2920 kg/m^3. The case with a homogeneous crust and mantle is shown as well as with a zoned upper mantle with a density equal to 3100 kg/m^3 just below the crust reaching the mantle value 10–20 km below. The mantle density depends very slightly on the core size and the figure here is for a core size of 350 km. Horizontal lines are mantle densities for different temperatures for model I. Best fit is in the range 800–900°C. The median sensitivity for density and inertia factor is about 350 km deep.

thickness of 70 km. For a PKT thickness of 30 km (our results), we find a mean thickness of 39 km. This mean thickness is 49.5 km when the PKT thickness is taken as 40 km (Khan et al.'s results [7]). For a crustal density of 2910 kg/m^3 and no transition zone, the mantle densities in these two cases range from 3332 kg/m^3 to 3334 kg/m^3 and from 3339 kg/m^3 to 3340 kg/m^3 respectively, depending on the core size (Fig. 7). These values are slightly sensitive to a transition zone, in which the density varies between 3100 kg/m^3 below the crust and the mantle density 10–20 km below. We now choose 3337 kg/m^3 for the mean mantle density.

Both seismic velocities and density can now be used to constrain the mantle temperature. Estimates are provided in Table 6, by computing the velocity shift necessary to explain the bulk velocities at depth in the range of 238–458 km and 458–738 km and the mean density in the mantle. By using velocities, this provides temperatures around 675°C and 950°C respectively at these depth ranges. We also find that model I fits twice better (in variance reduction) the density of the mantle than model II, even if the values correspond to a hotter temperature than for velocities, between 800°C and 900°C at about 350 km. Note here that model II is almost inconsistent for the joint interpretation of the velocities and density: velocities imply a colder mantle, while the density implies a hotter one. Fig. 8 shows that these temperatures correspond to the cold models found by Hood et al. [38], i.e. a mixture of 50% pyroxene and 50% olivine, which is quite comparable in Al_2O_3 to our model I. These temperatures are slightly smaller than the standard estimates, such as those proposed by Hood and

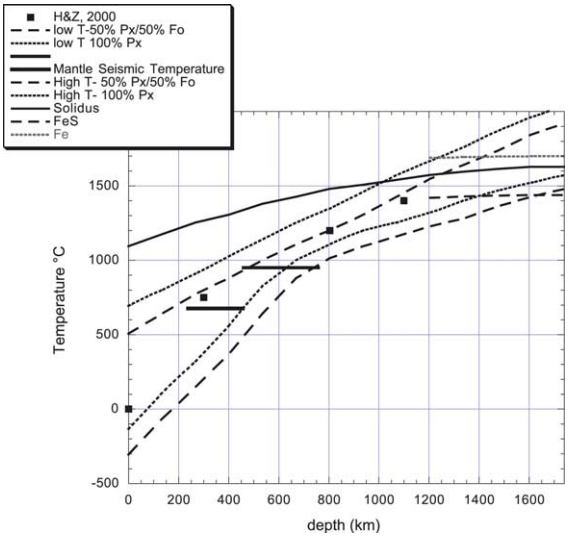

Fig. 8. Comparison of temperatures from this model and previous studies. The solid line is the solidus temperature of the mantle and the almost horizontal short dashed and long dashed lines indicate the melting temperature of Fe and Fe–S respectively. The square gives the temperature proposed by Hood and Zuber [10]. The short dashed curve gives the minimum and maximum range of temperature for a mantle model with a composition 50% Px and 50% Fo as proposed by Hood [9,38]. The two other long dashed curves are temperatures for a pure Px model. The horizontal black bar is the estimated temperature for two depth ranges.

Zuber [10]. These colder temperatures are more in accordance with other geophysical constraints, such as selenotherms obtained from the observed electrical conductivity of the Moon and inverted with aluminous orthopyroxenes [38] and low attenuation in the middle mantle [4,11]. They also favor mascon maintenance over 3–4 billion years [39] even if the latter can also be achieved with lower mantle viscosity due to the smaller planetary radius [40]. The increase of the temperature in the first 700 km can therefore be associated with the present thermal lithosphere of the Moon, possibly as thick as 700 km [41].

6. U content and Moon formation constraints

Let us now estimate the global U bulk content of the Moon with our crustal and mantle composition constraints. With the terranes approach of Jolliff et al. [16], a mean crustal abundance in Th of about 1.05 ppm, an average thickness of about 70 km and a lunar bulk crustal contribution of about 29 ppb were found for a Th/U ratio of 3.67. A new crustal thickness has a major effect on this budget and moreover the results will depend on the thicknesses of the upper and lower crust of Feldspathic Highland Terrane. If the crustal reduction is distributed in both layers equally, a PKT crustal thickness of 30 km leads to a bulk Th, mean crustal thickness and bulk U of 1.01 ppm, 39 km and 16 ppb respectively. For a 40 km thick PKT crust, closer to the value found by Khan et al., we get 1.03 ppm, 49.5 km and 20.4 ppb respectively. However, if the crustal thickness reduction affects mainly the lower crust, a lower bulk U is found due to the enrichment in Th of the lower crust compared to the upper one.

Another approach to estimate the bulk U of the mantle is to assume a C1 origin for the bulk Moon, and to assume no fractionation between Al_2O_3 and U [15]. A bulk U of 32 ppb is then obtained. However, a C1 origin, and more generally a pure chondritic origin, of the Moon is probably incompatible with the impact scenario, in which the Moon forms from a mixture of Earth's crust, Earth's upper mantle, proto-Moon mantle and proto-Moon core. During this impact, a large part of the Earth proto-crust, probably already differentiated, was likely to be ejected, leading to some enrichment in U.

The lunar mantle composition, however, gives some constraints on this early mixture, even if the results are model-dependent. For that purpose, let us assume that the Moon relative content F_X^{Mo} for the chemical species X, such as SiO_2, Al_2O_3, MgO, CaO and U is:

$$F_X^{Mo} = a\,F_X^{Ec} + b\,F_X^{Em} + c\,F_X^{MoP}$$

i.e. the sum of species from the Earth crust (F_X^{Ec}), the Earth mantle (F_X^{Em}) and the mantle of impactor (F_X^{MoP}), while the FeO content is provided by:

$$F_{FeO}^{Mo} = a\,F_{FeO}^{Ec} + b\,F_{FeO}^{Em} + c\,F_{FeO}^{MoP} + d$$

where a, b, c are the fractions of the Moon originating from the Earth crust, mantle, and impactor mantle, and d is the fraction of FeO in the Moon's mantle produced by a post-impact oxidation of iron from the impactor core. The rest of the impactor core is assumed to join the Earth or the lunar core. Let us now assume F_{FeO}^{I} fixed to the value of model I and determine the fractions of Earth crust, mantle and mantle impactor needed to explain the actual composition of the Moon upper mantle in SiO_2, Al_2O_3, MgO, CaO. These fractions a, b, and c will be found by a least square fitting of the computed values F_X^{Mo} with the values F_X^{I} of model I for the species SiO_2, Al_2O_3, MgO, and CaO. This leads to the minimization of C, defined as:

$$C = (F_{SiO_2}^{I} - F_{SiO_2}^{Mo})^2 + (F_{Al_2O_3}^{I} - F_{Al_2O_3}^{Mo})^2 + (F_{MgO}^{I} - F_{MgO}^{Mo})^2 + (F_{CaO}^{I} - F_{CaO}^{Mo})^2.$$

If we assume that all materials originate from these reservoirs, we have the supplementary constraint:

$$1 = a + b + c + d$$

The composition of the primitive Earth at the time of impact is poorly known and we assume a primitive tholeiitic crust (with either continental or oceanic composition), together with a residual

Table 7
Compositions of the different reservoirs used in the model after Anderson [42]

	Notation	SiO_2 (%)	Al_2O_3 (%)	FeO (%)	MgO (%)	CaO (%)	U (ppb)	Fe+Ni (%)
C1 chondrite	F^{MoP}	30.9	2.4	32.5	20.8	2	13	1.3
ES chondrite		39.1	1.9	1.7	21.3	1.6	9	28.4
Continental tholeiite	F^{Ec}	50.6	13.6	10	8.5	10	60–80	–
Oceanic tholeiite		50.7	15.6	9.9	7.7	11.4	60–80	–
Eclogite extract	F^{Em}	46.2	8.3	12.3	24.1	6.9	20	
Moon bulk model	F^{dat}	53.5	6.4	13.3	21.9	4.9		

upper mantle with a composition close to eclogite extract, as suggested by Anderson [42]. We consider two chondritic models for the proto-Moon, either carbonaceous (C1) or enstatite (ES). The compositions of the different reservoirs are given in Table 7. Generally our results show that the SiO_2 content is so low for C1 composition that the mixing coefficient found for minimizing C are unphysical, i.e. not in the range of [0–1]. A solution can be found only for an ES origin of the proto-Moon (Table 8). With about 8% enrichment in SiO_2, we can match the Moon bulk composition with 24% primitive Earth tholeiitic oceanic crust, 8% primitive Earth upper mantle based on eclogite extract and 67% associated with material originating from the proto-Moon (58% from the mantle with modified ES composition and 9% FeO related to oxidation of former core iron). An alternative is found if the primitive Earth crust is enriched in SiO_2. If the thickness of this Earth crust is about 40 km, this is equivalent to 35% of the Earth's crust. Several arguments support our proposal for such a proto-enstatite Moon: the obtained fractions having an Earth origin and proto-Moon origin are first comparable to those obtained by the simulation of an impact between a proto-Moon and an almost completely formed Earth [43]. In these experiments, the fraction of the orbiting mass originating from the impactor does indeed range from 0.6 to 0.9. Moreover, the analysis of these experiments has shown that about 30% (20%) of the topmost 30 km (75 km) of the proto-Earth was ejected beyond the Roche limit and was therefore re-accreted in the Moon (C. Fryer and W. Benz, personal communication). These values are close to our results.

We also found about 6% of iron originating from the proto-Moon core, a value reached for impact parameters higher than 0.85. Second, we have an almost perfect coincidence in ^{17}O and ^{18}O for enstatite chondrite with the Earth's and Moon's mantle [44]. Third, either a first stage of the accretion, for about 80% of the Earth's material [46], or the complete accretion [45,47] might be done with very reducing materials comparable

Table 8
Fractions of the different reservoirs for the Moon formation

ES non-SiO_2 fractionation	Continental tholeiites				Oceanic tholeiites			
	Earth crust	Earth mantle	Proto-Moon	Iron core	Earth crust	Earth mantle	Proto-Moon	Iron core
1	0.312	−0.087	0.685	0.089	0.284	−0.144	0.763	0.096
0.98	0.303	−0.028	0.638	0.087	0.275	−0.076	0.709	0.093
0.96	0.295	0.024	0.596	0.085	0.267	−0.02	0.66	0.09
0.94	0.287	0.069	0.56	0.083	0.26	0.03	0.618	0.088
0.92	0.281	0.109	0.528	0.0813	0.244	0.078	0.581	0.086
0.9	0.275	0.145	0.449	0.0798	0.248	0.118	0.549	0.0846

Case with an enstatitic chondritic Moon and with a fractionation of SiO_2 (from 0 to 10% depletion). The left four columns are for a proto-Earth crust with a composition given by continental tholeiites. The right four columns are for a proto-Earth with a composition given by oceanic tholeiites.

to enstatite. During that period, the Mars-sized impactor was probably already formed, as well as the central part of the Earth corresponding to the lower mantle, for which a good match of the isotopic composition of nitrogen with enstatite is likely, as reported for diamonds originating in the deep upper mantle and lower mantle [48].

With this model, the bulk U content is mainly related to the U enrichment of the tholeiitic primitive crust. Let us assume a bulk U of 20 ppb for the proto-Earth and 9 ppb for the enstatite bulk composition. Assuming a core mass of 30% for the Earth impactor, this yields about 14 ppb for the bulk mantle of the Earth impactor. The bulk U of the Moon is then found to be between 28 ppb and 33 ppb for a relative enrichment between 3 and 4 and no depletion of the primitive Earth mantle. With a depletion of 75%, we get between 25 and 31 ppb. In all cases, therefore, a *cosmochemical* mean value of about 28 ppb seems reasonable from a reservoir approach and is moreover coherent with the *geophysical* overall budget of U in the crust, depleted upper mantle and non-depleted lower mantle, based on more geophysical arguments related to heat flux. By taking 28 ppb and assuming known the amount of U in the crust from the terrane inventory and crustal thickness determination, we can now address the problem of the mantle depletion. The key parameter is the radius of the transition between the primitive and depleted mantle. The only seismic discontinuity is found at a depth of about 750 km, 200 km deeper that the 550 km interpreted in the Nakamura model [26] as the base of the primordial lunar magma ocean. However, as noted previously, this seismic discontinuity is very poorly constrained and is very likely both model- and data-dependent. Many recent studies, however, confirm that the Moon's initial state was very hot as a consequence of the large amount of energy released after the giant impact as well as the very rapid re-accretion rate of the lunatesimal. The depth of the magma ocean is then estimated to be between 500 and 1000 km. Let us therefore assume that the upper mantle is depleted to about 73%, as assumed by Binder and Lange [49], and that the lower mantle is undepleted. For an a posteriori U bulk of 28 ppb, we need a base of the magma ocean 760 km deep, with about 17 ppb in the crust, 6.2 ppb in the upper depleted mantle and 5.8 ppb in the lower undepleted mantle. A core was assumed here, with a radius of 300 km. The two different bulk U estimates therefore match nicely the different constraints of our model (crustal thickness, upper mantle composition and possible 750 km discontinuity). They are also close to the upper estimate of Rasmussen and Warren [12]. Much of this coherence is related to the crust thickness. A thicker crust of about 70 km, as previously considered, is indeed equivalent to more than 30 ppb of bulk U [15]. Such a thick crust, plus a shallow depth for the primitive magma ocean as for the Nakamura model [26], lead to an a posteriori bulk budget larger than 40 ppb, even with full depletion of the upper mantle in U, and therefore to inconsis-

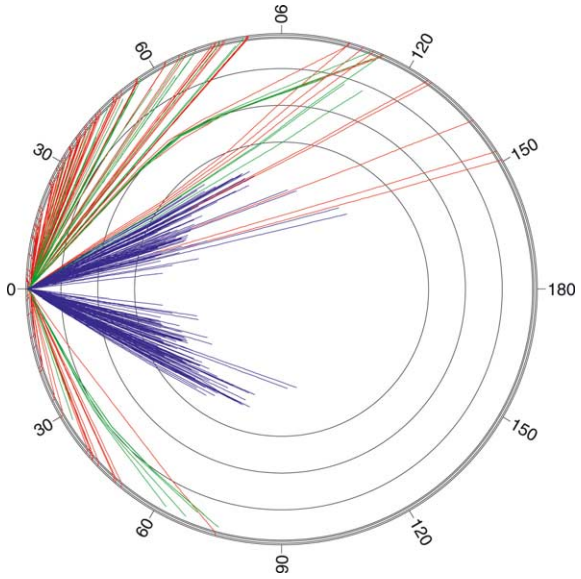

Fig. 9. A priori rays for the Nakamura model. Blue rays are for the deep events, red for the meteorite impacts and green for the shallow moonquakes. Only the rays corresponding to error bars less than 10 s are plotted. P wave rays are represented in the upper part, S waves in the lower one. Note that for impacts with epicentral distances greater than 90° only the P arrival times are useful for the inversion, therefore providing only one datum for the structure determination after localization of the impact. A total of 319 P and S arrival time data were used to constrain 59 seismic sources including 185 source parameters and 134 degrees of freedom available for internal structure constraints.

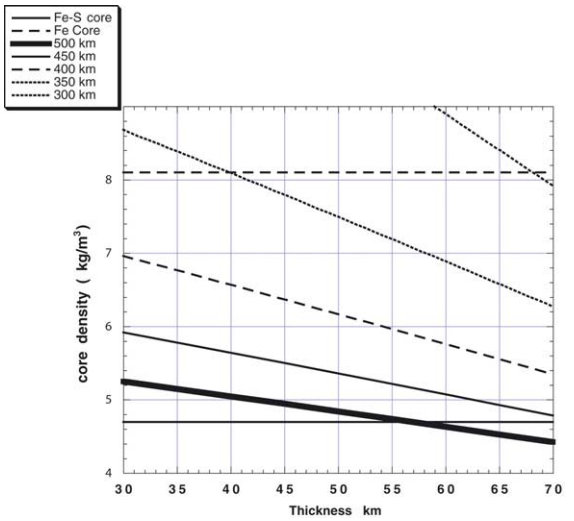

Fig. 10. Core density constraints for different thicknesses of the transition zone between the mantle and the crust with respect to the thickness of the crust. Several curves are shown for different core radii. The upper horizontal line matches the density of pure γ-Fe while the lower one is for density of Fe–S.

tencies between geophysical and geochemical data. Moreover, an enrichment of U during the Moon formation is then mandatory.

7. Indirect constraints on the core

As shown by Fig. 9, our seismic model does not constrain the core directly: this seismic determination needs seismic phases traveling through the core, which will hopefully be first recorded by Lunar A [24]. However, by providing both the seismic determination of the crustal thickness and indirect mantle and crust densities, through mineralogical hypotheses, we can constrain the mass of the core. The range of models is shown in Fig. 10. Estimates based on the lunar induced magnetic moment in the geomagnetic tail [10] provide a core radius of 340 ± 90 km. For a density of 2910 kg/m^3 in the crust and a 20 km transition zone where density increases from 3100 kg/m^3 to the mantle value, we find a density between 6400 kg/m^3 and 6600 kg/m^3 for a 400 km core, i.e. about 50% FeS and 50% Fe in composition. Only the core mass is constrained: pure γ-Fe core composition leads to a core size of about 330–350 km while Fe–S leads to about 500–550 km, with a radius slightly less than the size proposed by Kuskov and Kronrod [50]. Increasing the thickness of the transition zone reduces the core mass.

Fig. 8 shows that the extrapolation of the mantle temperatures toward the center of the Moon is compatible with a Fe–S liquid core, necessary to explain lunar ranging data [51]. Temperatures much higher than the solidus and/or necessary for a liquid pure iron core are incompatible with our model. If the core is fully liquid, a rather large core is therefore likely even if a more complex mantle structure, especially with a mantle density gradient between the upper and lower mantle, could lower its size.

8. Conclusion

We presented a new lunar model based on the arrival times of P and S waves from about 60 deep and shallow lunar quakes and surface impacts. It provides a new estimate of the crustal thickness, in the range of 30 ± 2.5 km, on the PKT leading to a mean crustal thickness of 40 km with a density of 3320 kg/m^3. With a completely independent set of travel times, this therefore confirms other recent studies [6–8] pointing to a thinner crustal thickness. We also propose a lunar mantle dominated by a temperature increase reaching about 700°C and 900°C at depths of 350 km and 600 km respectively. In the upper mantle of the Moon, at depth around 350 km, we find shear velocities of 4.5 ± 0.150 km/s and 7.75 ± 0.150 km/s.

The mantle velocities and density fit with a pyroxenite mantle. Together with an anorthosite crust of 40 km, we find a bulk composition of the Moon's mantle+crust of 53.5% SiO_2, 6.4% Al_2O_3, 13.3% FeO, 21.9% MgO and 4.9% CaO. This composition can be explained by the collision between the primitive Earth and an impactor with a composition close to enstatite chondrites. For example, a bulk Moon constituted of about 28% primitive Earth tholeiitic crust, 10% primitive eclogite extract originating from the primitive

mantle, 53% impactor mantle and 8% impactor Fe core fits the lunar upper mantle composition. A slight enrichment in SiO_2 is needed, either from the impactor enstatite reservoir or from the primitive Earth crustal reservoir. Such a model implies a tangential impact, in order to put in orbit enough iron from the impactor. The water necessary for oxidation of the iron is found to be small compared to the water available in both the Earth ejecta and proto-impactor ejecta.

Lastly, we propose a bulk U content of 28 ppb, compatible with those obtained either from an inventory of the source of U in the different reservoirs participating in the formation of the Moon or from an inventory of the present U in both the crust, depleted upper mantle and a depleted lower mantle having its base at a depth of 760 km.

Acknowledgements

This work was supported by the Programme National de Planétologie from INSU, by the French Space Agency, in the framework of a CNES/ISAS co-Is exchange program between the NetLander and Lunar A missions and by IUF grants. We thank Prof. Mizutani and ISAS for having transferred the complete set of Apollo data on modern support and L. Vinnik for pointing out the receiver function approach. We thank V. Dehant, M. Wieczorek, M. Javoy for comments, and R. Taylor and an anonymous referee for their review. This paper was finalized while one of us (P.L.) was at the Miller Institute for Basic Research in Science, UC Berkeley. This is IPGP contribution 1910.*[BW]*

References

[1] D.J. Lawrence, W.C. Fledman, B.L. Barraclough, A.B. Binder, R.C. Elphic, S. Maurice, M.C. Miller, T.H. Prettyman, Thorium abundances on the lunar surface, J. Geophys. Res. 105 (2000) 20307–20331.

[2] W.C. Feldman, O. Gasnault, S. Maurice, D.J. Lawrence, R.C. Elphic, P.G. Lucey, A.B. Binder, Global distribution of Lunar composition: New results from Lunar Prospector, J. Geophys. Res. 107 (2002) 5–14.

[3] A.S. Konopliv, A.B. Binder, L.L. Hood, A.B. Kucinskas, W.L. Sjogren, J.G. William, Improved gravity field of the Moon from Lunar Prospector, Science 281 (1998) 1476–1479.

[4] M.N. Toksöz, A.M. Dainty, S.C. Solomon, K.A. Anderson, Structure of the Moon, Rev. Geophys. Space Phys. 12 (1974) 539–567.

[5] N.R. Goins, A.M. Dainty, N. Toksoz, Structure of the Lunar highlands site Apollo 16, Geophys. Res. Lett. 8 (1981) 29–32.

[6] A. Khan, K. Mosegaard, K.L. Rasmussen, A new seismic velocity model for the Moon from a Monte Carlo inversion of the Apollo lunar seismic data, Geophys. Res. Lett. 27 (2000) 1591–1594.

[7] A. Khan, K. Mosegaard, An inquiry into the lunar interior – A non-linear inversion of the Apollo seismic data, J. Geophys. Res. 107 (2002) 1–23.

[8] H. Chenet, J. Gagnepain-Beyneix, P. Lognonné, L. Vinnik, Reprocessing of the Apollo lunar seismic data: A thinner lunar crust, EOS Trans. AGU 81 (2000) F771.

[9] L.L. Hood, Geophysical constraints on the Lunar interior, in: W.K. Hartmann, R.J. Philips, G.J. Taylor (Eds.), Origin of the Moon, Lunar and Planetary Institute, Houston, TX, 1986, pp. 361–410.

[10] L.L. Hood, M.T. Zuber, Geophysical constraints on the Lunar origin and evolution, in: R.M. Canup, K. Righter (Eds.), Origin of the Earth and Moon, Lunar and Planetary Institute, Houston, TX, 2000, pp. 397–409.

[11] P. Lognonné, B. Mosser, Planetary seismology, Surv. Geophys. 14 (1993) 239–302.

[12] K.L. Rasmussen, P.H. Warren, Megaregolith thickness, heat flow and the bulk composition of the Moon, Nature 313 (1985) 121–124.

[13] M.T. Zuber, D.E. Smith, F.G. Lemoine, G.A. Neumann, The shape and internal structure of the Moon from the Clementine mission, Science 266 (1994) 1839–1843.

[14] M.J. Drake, Is lunar bulk material similar to Earth's mantle, in: W.K. Hartmann, R.J. Phillips, G.J. Taylor (Eds.), Origin of the Moon, Lunar and Planetary Institute, Houston, TX, 1986, pp. 105–124.

[15] S.R. Taylor, The origin of the Moon: geochemical considerations, in: W.K. Hartmann, R.J. Phillips, G.J. Taylor (Eds.), Origin of the Moon, Lunar and Planetary Institute, Houston, TX, 1986, pp. 125–143.

[16] B.L. Jolliff, J.J. Gillis, L.A. Haskin, R.L. Korotev, M.A. Wieczorek, Major lunar crustal terranes: Surface expression and crust mantle origins, J. Geophys. Res. 105 (2000) 4197–4216.

[17] S.C. Solomon, J. Chaikin, Thermal expansion and thermal stress in the Moon and terrestrial planets: Clues to early thermal history, Proc. Lunar Sci. Conf. 7 (1976) 3229–3243.

[18] R.L. Kirk, D.J. Stevenson, The competition between thermal contraction and differentiation in the stress history of the moon, J. Geophys. Res. 94 (1989) 12133–12144.

[19] P.D. Spudis, P.A. Davis, A chemical and petrological model of the lunar crust and implication for lunar crustal

origin, J. Geophys. Res. 17 (Suppl. Lunar Planet. Sci. Conf. Proc.) (1986) E84–E90.
[20] P.D. Spudis, B.R. Hawke, P.G. Lucey, G.J. Taylor, K.R. Stockstill, Composition of the ejecta deposits of selected lunar basins from Clementine elemental maps, Lunar Planet. Sci. Conf. Abstr. 27 (1996) 1255–1256.
[21] M.A. Wieczorek, M.T. Zuber, The composition and origin of the lunar crust: Inferences from central peaks and geophysical crustal thickness modelling, Geophys. Res. Lett. 28 (2001) 4023–4026.
[22] M.A. Wieczorek, R.J. Phillips, Potential anomalies on a sphere: Application to the thickness of the lunar crust, J. Geophys. Res. 103 (1998) 1715–1724.
[23] L. Vinnik, H. Chenet, J. Gagnepain-Beyneix, P. Lognonné, First seismic receiver functions on the Moon, Geophys. Res. Lett. 28 (2001) 3031–3034.
[24] H. Mizutani, Lunar interior exploration by Japanese lunar penetrator mission, Lunar-A, J. Phys. Earth 43 (1995) 657–670.
[25] D. Lammlein, Lunar seismicity and tectonics, Phys. Earth Planet. Inter. 14 (1977) 224–273.
[26] Y. Nakamura, Seismic velocity structure of the lunar mantle, J. Geophys. Res. 88 (1983) 677–686.
[27] N.R. Goins, A.M. Dainty, M.N. Toksöz, Lunar seismology, the internal structure of the Moon, J. Geophys. Res. 86 (1981) 5061–5074.
[28] H. Wang, T. Todd, D. Richter, G. Simmons, Elastic properties of plagioclase aggregates and seismic velocities in the Moon, Geochim. Cosmochim. 3 (Suppl. 5, Proc. 4th Lunar Sci. Conf.) (1973) 1663–1672.
[29] H. Mizutani, M. Osako, Elastic waves velocities and thermal diffusivities of Apollo 17 rocks and their geophysical implications, Geochim. Cosmochim. 4 (Suppl. 5, Proc. 4th Lunar Sci. Conf.) (1974) 2891–2901.
[30] G. Simmons, T. Todd, H. Wang, The 25-km discontinuity: Implications for lunar history, Science 182 (1973) 158–161.
[31] O.L. Kuskov, Constitution of the Moon: 3. Composition of middle mantle from seismic data, Phys. Earth Planet. Inter. 90 (1995) 55–74.
[32] J.W. Morgan, J. Hertogen, E. Anders, The Moon: composition determined by nebula processes, Moon Planets 18 (1978) 465–478.
[33] J.H. Jones, J.W. Deleno, A three component model for the bulk composition of the Moon, Geochim. Cosmochim. Acta 53 (1989) 513–527.
[34] A.E. Ringwood, T. Irifune, Nature of the 650 km discontinuity: implication for mantle dynamics and differentiation, Nature 331 (1988) 131–136.
[35] A.E. Ringwood, E. Essene, Petrogenesis of Apollo 11 basalts, internal composition and origin of the Moon, Geochim. Cosmochim. Acta 34 (Apollo 11 Lunar Sci. Conf. Proc.) (1970) 769–799.
[36] J.H. John, L.L. Hood, Does the Moon have the same chemical composition as the Earth's upper mantle? in: H.E. Newsom, J.H. Jones (Eds.), Origin of the Earth, Oxford University Press, New York, 1990, pp. 85–98.
[37] S. Mueller, G.J. Taylor, R. Phillips, Lunar composition: A geophysical and petrological synthesis, J. Geophys. Res. 93 (1988) 6338–6352.
[38] L.L. Hood, F. Herbert, C.P. Sonett, Further efforts to limit lunar internal temperatures from electrical conductivity determinations, J. Geophys. Res. 87 (13th Lunar Planet. Sci. Conf. Proc.) (1982) A109–A116.
[39] S. Pullan, K. Lambeck, On constraining lunar mantle temperatures from gravity data, Lunar Planet. Sci. Conf. Proc. 11 (1980) 2031–2041.
[40] S. Zhong, M.T. Zuber, Long-wavelength topographic relaxation for self-gravitating planets and implications for the time-dependent compensation of surface topography, J. Geophys. Res. 105 (2000) 4153–4164.
[41] W. Konrad, T. Spohn, Comparative studies of the Moon and Mercury, Adv. Space Res. 19 (1997) 1511–1521.
[42] D. Anderson, Theory of the Earth, Blackwell, Boston, MA, 1989, pp. 17 and 223.
[43] R.M. Canup, E. Asphaug, Origin of the Moon in a giant impact near the end of the Earth's formation, Nature 412 (2001) 708–712.
[44] R.N. Clayton, T.K. Mayeda, Oxygen isotopic compositions of chondrites and aubrites, J. Geophys. Res. 89 (1984) C245–C249.
[45] M. Javoy, The integral enstatite chondrite model of the earth, Geophys. Res. Lett. 22 (1995) 2219–2222.
[46] H. Wänke, Constitution of terrestrial planets, Phil. Trans. R. Soc. London 303 (1981) 287–302.
[47] M. Drake, K. Righter, Determining the composition of the Earth, Nature 416 (2002) 39–44.
[48] M. Javoy, F. Pineau, Carbon and nitrogen isotopes in the mantle, Chem. Geol. 57 (1986) 41–62.
[49] A.B. Binder, M.A. Lange, On the thermal history, thermal state, and related tectonism of a moon of fission origin, J. Geophys. Res. 85 (1980) 3194–3208.
[50] O.L. Kuskov, V.A. Kronrod, Constitution of the Moon 5. Constraints on composition, density, temperature and radius of a core, Phys. Earth Planet. Inter. 107 (1998) 285–306.
[51] J.G. Williams, D.H. Boogs, C.F. Yoder, J.T. Racliff, J.O. Dickey, Lunar rotational dissipation in solid body and molten core, J. Geophys. Res. 106 (2001) 27933–27968.